

Demagnetization Detection in PMSMs Using Search Coils Exploiting Machine's Symmetry

Marcos Orviz Zapico
University of Oviedo. Dept of Elect.
Computer & System Engineering,
Gijón, 33204, Spain
orvizmarcos@uniovi.es

David Díaz Reigosa
University of Oviedo. Dept of Elect.
Computer & System Engineering,
Gijón, 33204, Spain
diazdavid@uniovi.es

Hyeon Jun Lee
Korea University. Department of
Electrical Engineering,
Seoul, Korea
lhjoon14@gmail.com

Muhammad Saad Rafaq
Korea University. Department of
Electrical Engineering,
Seoul, Korea
m.saadrafaq@gmail.com

Sang Bin Lee
Korea University. Department of
Electrical Engineering,
Seoul, Korea
sangbinlee@korea.ac.kr

Fernando Briz del Blanco
University of Oviedo. Dept of Elect.
Computer & System Engineering,
Gijón, 33204, Spain
fernando@isa.uniovi.es

Abstract— Magnet demagnetization in permanent magnet synchronous machines (PMSMs) can produce inadmissible performance degradation. Search coils (SCs) have been proven to be a viable option for its detection. Limitations of existing methods using SCs include the low sensitivity and the need of a large number of SCs. This paper proposes two methods for demagnetization detection of PMSMs using SCs which overcome these limitations. Zero-sequence voltage-based method relies on the zero-sequence voltage of three SCs electrically shifted 120 electrical degrees. On the other hand, differential voltage-based method computes the difference between the voltage induced in SCs with the same electrical angle, i.e., both SCs are electrically shifted 360°.¹

Keywords— Permanent magnet, demagnetization, search coil, zero-sequence voltage, differential voltage

I. INTRODUCTION

Permanent magnet synchronous machines (PMSMs) are the preferred solution in many applications like hybrid and electric vehicles (HEVs, EVs), wind generation, servodrives, etc. owing to their high power and torque densities, high efficiency, and good controllability. Drive reliability is critical for many applications, development of condition monitoring and fault detection methods have received significant attention over the last years [1]-[17]. Motor current signature analysis (MCSA) [1], [2], Hall-effect sensors [3]-[6], use of high frequency signals (HFI) [7]-[10], and

search coils (SCs) in the stator slots [11]-[17] have been proposed for this purpose. Table I summarizes the main properties of existing techniques for the particular case of PM demagnetization detection. MCSA relies on specific harmonics in the stator current spectrum. However, other types of faults producing asymmetries in the rotor (partial demagnetization, dynamic / static eccentricity, misalignment, etc.) produce identical harmonic components at the same frequencies, leading to high levels of uncertainty in the fault detection. Injection of a HF signal in the stator terminals produces some adverse effects during the normal operation of the machine (e.g., additional losses, vibrations, and noise), and its performance highly depends on machine's parameters. Hall-effect sensors measure the PM field at a specific point, leakage flux measurements being sensible to sensor position and orientation. SCs overcome most of these limitations as (i) the voltage induced in a SC allows to detect rotor asymmetries, (ii) injection of additional signals is not required, (iii) is independent of the machine parameters and (iv) they provide a direct measurement of the air gap flux. However, SCs are invasive and operation at low speeds or standstill is not possible.

Table II summarizes the methods based on SCs reported in the literature for different monitoring and diagnosis purposes, including the number of SCs being required. It is seen that the methods reported for PM demagnetization detection require one

Table I: Comparative analysis of fault detection techniques

	MCSA [1],[2]	Hall-Effect [3]-[6]	HFI [7]-[10]	SCs [11]-[17]
Sensor cost	✓	✓	✓	✓
Invasive	✓	✗	✓	✗
Whole speed range	✗	✓	✓	✗
Parameter sensitivity	✓	✓	✗	✓
Computational burden	✗	✓	✗	✓

Table II: Fault detection techniques based on SCs

Number of SCs	Static Eccentricity	Dynamic Eccentricity	Interturn Short-circuit	PM Demagnetization
12 (one per slot) [12]	✓	✓	✓	✓
54 (one per slot) [13]	✗	✗	✓	✓
2 [14]	✓	✓	✗	✗
3 [15]	✓	✗	✗	✗
1 (around 3 teeth) [16]	✗	✓	✗	✗
1 (around 5-10 teeth) [17]	✗	✗	✓	✗

¹ This work was supported in part by the Research, Technological Development and Innovation Programs of the Spanish Ministry of Science and Innovation, under grant PID2019-106057RB-I00.

SC per slot [12], [13]. These methods track incremental variations of the fundamental component of the induced voltage in the SC. However, establishing a relationship between the induced voltage and the magnetization state is not trivial, due to the influence of several factors as speed, torque level, etc. Defining a fault indicator which is equal to zero when the machine is healthy and increases proportionally to demagnetization level would be therefore desirable.

This paper proposes two different implementations for demagnetization detection in PMSMs using SCs which fulfil such requirement:

- Zero-sequence voltage-based
- Differential voltage-based.

The most evident difference between these two methods is that the differential voltage approach requires two sensors, while the zero-sequence approach requires three sensors. However, it will be shown that the feasibility of these two methods also depends on machine design parameters, the most relevant being number of stator slots and rotor poles.

The paper is organized as follows: Section II describes the machine design and the SCs arrangement. Section III introduces the proposed PM demagnetization fault detection techniques and studies the viability of the methods depending on the machine configuration. Section IV develops a model for harmonic prediction based on Fourier series analysis. Fault detection and quantification process is presented in Section V. Section VI focuses on data processing. Section VII provides FEA simulation results. Conclusions are finally given in Section VIII.

II. MACHINE DESIGN AND SEARCH COIL ARRANGEMENT

Table III shows the main characteristics of the IPMSM test machine. FEM model and a picture of the machine are shown in Fig. 1. The machine is equipped with 4 SCs that will be combined as follows:

- Zero-sequence voltage based demagnetization detection requires three SCs shifted 120 electrical degrees: SC-1, SC-2, and SC-3 in Fig. 1 will be used therefore.
- Differential voltage based demagnetization detection measures the differences between two poles and

Machine type	IPMSM
Number of slots	9
Number of poles	6
Rated Current	12 A
Number of turns/SC	10

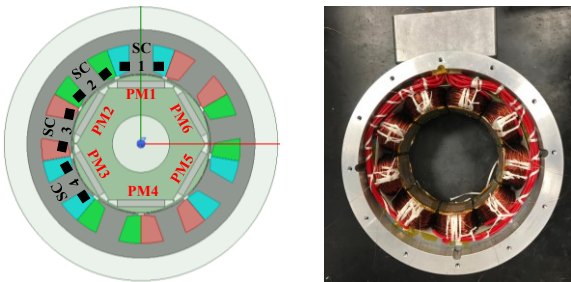


Fig. 1: FEA model of the test machine and stator of the test machine including the SCs.

requires therefore two SCs shifted 360 electrical degrees: SC-1 and SC-4 in Fig. 1 will be used.

III. VIABILITY OF THE PROPOSED METHODS

The aim of the two methods that are proposed is to provide a signal which is zero when the machine is healthy and increases proportionally to the demagnetization level.

A. Zero-Sequence Voltage Based Implementation

The zero-sequence voltage component resulting from three SCs that are shifted by 120 electrical degrees is defined as (1), where V_{SC1} , V_{SC2} and V_{SC3} are the induced voltages in each SC (see SC-1, SC-2 and SC-3 in Fig. 1).

$$V_0 = 1/3 \cdot (V_{SC1} + V_{SC2} + V_{SC3}) \quad (1)$$

In a perfectly balanced machine, V_0 will be zero. Asymmetric PM demagnetization will result in a voltage unbalance, that will be reflected in the zero sequence voltage, V_0 , and which will increase proportionally to the level of asymmetry. Furthermore, the harmonic components of the zero-sequence voltage will be shown to provide information about the type of demagnetization fault. This method can be only applied in machines with stator teeth phase shifted 120 electrical degrees.

B. Differential Voltage Based Implementation

The induced voltage in two SCs located 360 electrical degrees from each other (see SC-1 and SC-4 in Fig. 1) will be identical for the case of a perfectly balanced machine. The differential voltage can be used therefore as a metric of demagnetization. This approach only requires two sensors but has the drawback that it can only be applied to machines having stator teeth 360° electrical degrees phase shifted.

C. Feasibility Depending on the Machine Configuration

From the previous discussion it is clear that the feasibility of both the zero-sequence voltage-based and the differential voltage-based methods depends on the machine configuration. Then, the viability of both methods to be applied depending on the machine number of stator slots and pole pairs will be analyzed.

Equation (2) provides the number of slots between two slots electrically shifted 120°, n_{120} , which is seen to be a function of the number of stator slots, n_s and the number of pole pairs, P . k is an iterative constant ($k = 0, 1, 2, 3 \dots$) that increases its value until an integer value of n_{120} that fulfils $1 < n_{120} < n_s$ is reached. If no integer value of n_{120} fulfils the mentioned conditions, such machine design is not suitable for the use of the zero-sequence voltage. Similarly, equation (3) provides the number of stator slots between two slots electrically shifted 360°.

$$n_{120} = \frac{n_s}{P} (k \pm 1/3) \quad (2) \quad n_{360} = \frac{n_s}{P} k \quad (3)$$

From (2) and (3), it is possible to obtain the combinations of stator slots and rotor poles which allow the implementation of the zero-sequence voltage-based (see Table IV) and the differential voltage-based (see Table V) demagnetization detection.

It is observed from Table IV that the zero-sequence voltage-based cannot be used in several configurations with a number of pole pairs being an integer multiple of 3. Interestingly, Table V shows that the differential voltage-based method is feasible for all machine designs for which the zero-sequence voltage based option is not viable. Thus,

at least one of the methods proposed in this paper can be used for any machine design configurations shown in Tables IV and V.

		Pole Pairs (P)								
		2	3	4	5	6	7	8	9	10
Stator Slots (n_s)	3	Green								
	6	Green	Red	Green						
	9	Green				Green				
	12	Green	Red			Red	Green	Green		
	15	Green	Red			Red			Red	Green
	18	Green							Red	Red
	21	Green	Red			Red			Red	Green
	24	Green							Red	Red
	27	Green								
	30	Green	Red			Red			Red	Red
	33	Green							Red	Red
	36	Green								
	39	Green	Red			Red			Red	Red
	42	Green							Red	Red
	45	Green	Red			Red			Red	Red
48	Green	Red			Red			Red	Red	

		Pole Pairs (P)								
		2	3	4	5	6	7	8	9	10
Stator Slots (n_s)	3	Red								
	6	Green	Green	Green						
	9	Red		Red	Red	Green				
	12	Green		Green	Red	Green	Red	Green		
	15	Red		Red			Red	Red	Green	Green
	18	Green			Red		Red	Red		
	21	Red		Red			Green	Red	Red	Red
	24	Green			Red		Red	Red		Green
	27	Red		Red			Red	Red	Red	Red
	30	Green								
	33	Red		Red			Red	Red	Red	Red
	36	Green			Red		Red	Red		
	39	Red		Red			Red	Red	Red	Red
	42	Green			Red		Green	Red		
	45	Red		Red			Red	Red	Red	Red
48	Green			Red		Red	Red			

Green cells: feasible designs; red cells: unfeasible designs; white cells: cannot be built (slot/pole/phases ratio lower than 0.25).

IV. HARMONIC CONTENT OF ZERO-SEQUENCE AND DIFFERENTIAL VOLTAGE

In the previous section, two methods for demagnetization fault detection using SCs have been presented; constructive limitations of each method have been also reported. The harmonic content of both the differential voltage and the zero-sequence voltage when a PM suffers a demagnetization fault depends on the machine stator slots and rotor poles. Therefore, in this section a model to predict the zero-sequence and differential voltage harmonic components when a partial demagnetization

fault occurs in one PM depending on the machine number of stator slots and rotor poles will be developed.

Fig. 2a shows the ideal induced voltages in three SCs electrically shifted 120 electrical degrees. Fig. 2b shows the zero-sequence voltage, V_0 . If one of the PMs suffers a partial demagnetization, the voltage induced in the search coils will not be sinusoidal anymore, but shaped by the demagnetized PM.

The effect of the demagnetized magnet on the induced voltage will be modelled as the product of the sinusoidal waveforms and a window function (see Fig. 2c [4]), see Fig. 2d. It is noted that more elaborated window functions could be defined based on the knowledge of demagnetization patterns, stator and rotor design (e.g., magnet shape, magnet layers, flux barriers, stator teeth design, etc.). This is a subject of ongoing research. The resulting zero-sequence voltage is shown in Fig. 2e. Finally, the harmonic components of the zero-sequence voltage after the demagnetization fault can be seen in Fig. 2f (being the electrical frequency the fundamental one).

Similarly, Fig. 3a shows the ideal induced voltages in two SCs electrically shifted 360 electrical degrees. Fig. 3b shows the differential voltage, V_{diff} . The corresponding window functions are represented in Fig. 3c. Fig. 3d and 3e show the induced voltage in the SCs and the resulting differential voltage including the effect of the demagnetized magnet, respectively. Finally, the harmonic components of the differential voltage after the demagnetization fault can be seen in Fig. 3f.

The zero-sequence voltage is built from the addition of three signals which result from the product of three sinusoidal signals and three window signals electrically shifted 120 degrees, Fig. 2. The contribution of the three sinusoidal signals, 120 electrical degrees phase shifted, on the zero-sequence voltage is null. Therefore, the harmonics of the zero-sequence voltage will result from the window signal. The same conclusions hold for the differential voltage. Then, the harmonic components of the zero-sequence voltage will result from the addition of the three window signals electrically shifted θ_{w0} (see (4)). On the other hand, the harmonic components of the differential voltage will result from the addition of two window signals electrically shifted θ_{wd} (see (5)). The angle between window signals (θ_{w0} for the zero-sequence voltage and θ_{wd} for the differential voltage) depends on n_{120} (for the zero-sequence voltage) and n_{360} (for the differential voltage).

$$\theta_{w0} = \frac{2\pi}{n_s} n_{120} \quad (4)$$

$$\theta_{wd} = \frac{2\pi}{n_s} n_{360} \quad (5)$$

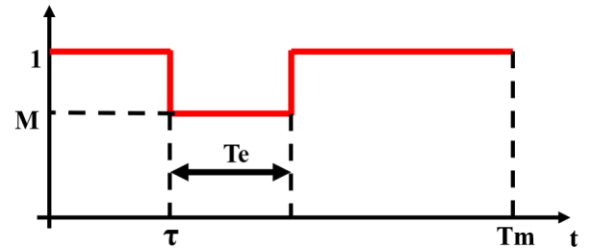


Fig. 4: Window function for PM demagnetization (1 PM demagnetized) depending on the mechanical and the electrical period, T_m and T_e , the time instant in which the demagnetized PM reduces the SC voltage, τ and the demagnetization level, M .

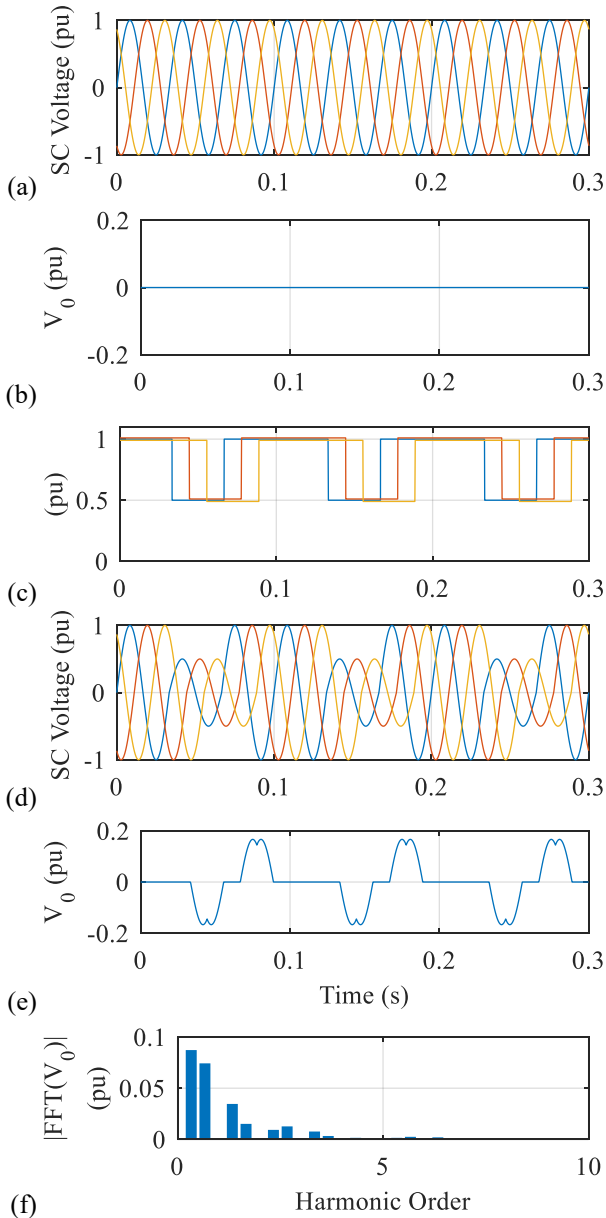


Fig. 2: (a) Ideal SC voltages (p.u.) in a healthy machine, (b) zero-sequence SC voltage, (c) profile of SC voltage variation due to PM demagnetization (1 PM demagnetized), (d) modeled SC voltages due to demagnetization obtained multiplying the theoretical SC voltages in (a) by the window functions in (c), (e) zero-sequence SC voltage resulting from the SC voltages in (d), and (f) FFT of the zero-sequence voltage shown in (e). $I_{dq} = \mathbf{0}$ p.u., $\omega_r = \mathbf{1}$ p.u.

It can be deduced from the previous discussion that the harmonic components of both the zero-sequence and the differential voltage will be the ones of a single window signal unless those components that are cancelled due to the addition of the three window signals for the zero-sequence voltage and the subtraction of the two window signals for the differential voltage.

Fourier series can be used to predict the amplitude and phase of the harmonic components of the window signal in Fig. 4, mathematically defined by (6), where T_e is the electric period, T_m is mechanical period, and τ the time instant in which the SC voltage begins to be affected by the demagnetized PM.

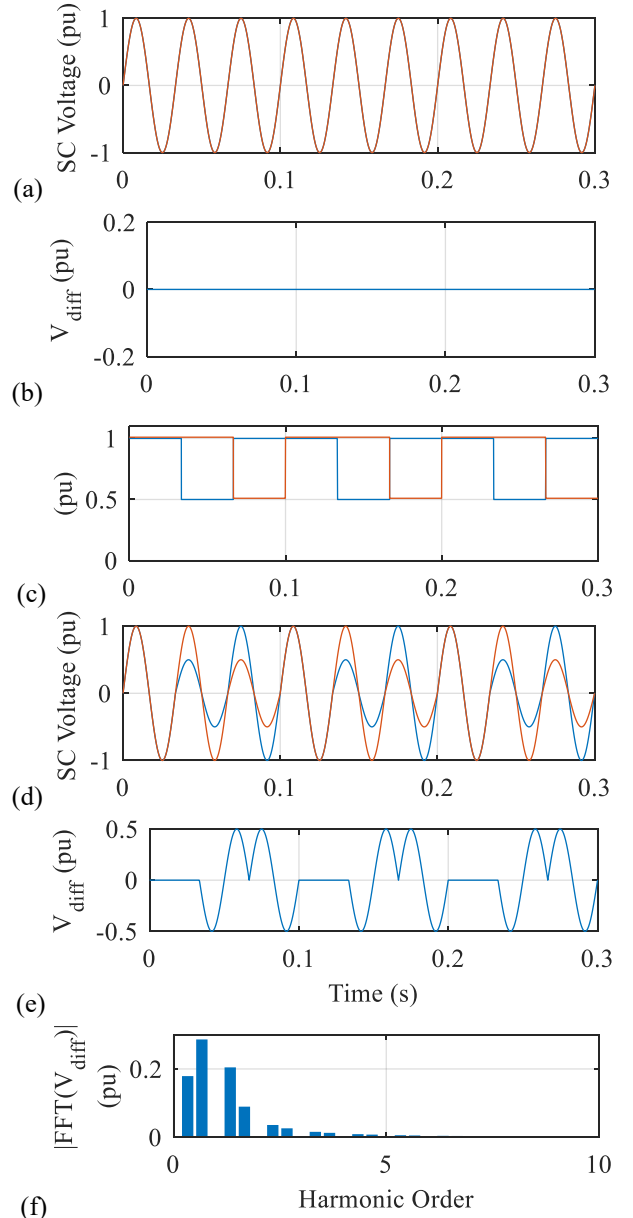


Fig. 3: (a) Theoretical SC voltages (p.u.) in a healthy machine, (b) differential SC voltage, (c) profile of SC voltage variation due to PM demagnetization (1 PM demagnetized), (d) modeled SC voltages due to demagnetization obtained multiplying the theoretical SC voltages in (a) by the window functions in (c), (e) differential SC voltage resulting from the SC voltages in (d), and (f) FFT of the differential voltage shown in (e). $I_{dq} = \mathbf{0}$ p.u., $\omega_r = \mathbf{1}$ p.u.

$$s(t) = \begin{cases} 1 \rightarrow & 0 < t < \tau \\ M \rightarrow & \tau < t < \tau + T_e \\ 1 \rightarrow & \tau + T_e < t < T_m \end{cases}, \quad (6)$$

Fourier series of a signal, $y(t)$, is defined by (7)-(10), where $a(0)$, $a(n)$ and $b(n)$ are the so-called Fourier coefficients, T is the period of function $y(t)$, t is the time, and n represents the harmonic component order (the mechanical frequency of the machine being the fundamental one).

$$y(t) = \frac{a(0)}{2} + \sum_{n=1}^{\infty} \left[a(n) \cos\left(\frac{2\pi n}{T} t\right) + b(n) \sin\left(\frac{2\pi n}{T} t\right) \right] \quad (7)$$

$$a_{(0)} = \frac{2}{T} \int_0^T s(t) dt \quad (8)$$

$$a_{(n)} = \frac{2}{T} \int_0^T s(t) \cos\left(\frac{2\pi n}{T} t\right) dt \quad (9)$$

$$b_{(n)} = \frac{2}{T} \int_0^T s(t) \sin\left(\frac{2\pi n}{T} t\right) dt \quad (10)$$

If $y(t) = s(t)$, (11)-(13) are obtained.

$$a_{(0)} = \frac{2}{T_m} [T_e(M-1)] \quad (11)$$

$$a_{(n)} = \frac{(M-1)}{\pi n} \left[\sin\left(\frac{2\pi n(T_e + \tau)}{T_m}\right) - \sin\left(\frac{2\pi n\tau}{T_m}\right) \right] \quad (12)$$

$$b_{(n)} = \frac{(M-1)}{\pi n} \left[\cos\left(\frac{2\pi n\tau}{T_m}\right) - \cos\left(\frac{2\pi n(T_e + \tau)}{T_m}\right) \right] \quad (13)$$

The amplitude and phase of each harmonic component is defined by (14) and (15) respectively; (16) and (17) being obtained by substituting (11)-(13) into (14)-(15).

$$|Y(n)| = \sqrt{a_{(n)}^2 + b_{(n)}^2} \quad (14)$$

$$\phi(n) = \arctan\left(-\frac{b_{(n)}}{a_{(n)}}\right) \quad (15)$$

$$|Y(n)| = \left| \frac{M-1}{\pi n} \sqrt{2 \left[1 - \cos\left(\frac{2\pi n}{P}\right) \right]} \right| \quad (16)$$

$$\phi(n) = \begin{cases} -\frac{\pi n}{T_m} (2\tau + T_e) + \pi \rightarrow k_1 P < n < k_2 P \\ -\frac{\pi n}{T_m} (2\tau + T_e) \rightarrow k_2 P < n < (k_1 + 2) P \end{cases} \quad (17)$$

where $k_1 = 0, 2, 4, 6 \dots$ and $k_2 = 1, 3, 5, 7 \dots$

Equations (16) and (17) allow to predict both the amplitude and the phase of each harmonic component of a single window signal, $s(t)$. Some of these harmonic components will be cancelled in both the zero-sequence and the differential voltage. (18) and (19) indicate if a harmonic component, n , of the single window signal would be cancelled in the zero-sequence voltage or the differential voltage, respectively.

$$\phi_1 - \phi_2 = \Delta\phi(n) = -\frac{2\pi n}{T_m} (\tau_1 - \tau_2) = \pm 120^\circ \quad (18)$$

$$\phi_1 - \phi_2 = \Delta\phi(n) = -\frac{2\pi n}{T_m} (\tau_1 - \tau_2) = 0^\circ \quad (19)$$

where $\tau_1 - \tau_2$ is the time lag between two window signals, which can be obtained from the phase shift defined in (4) and (5). Therefore, equations (18) and (19) can be rewritten as (20) and (21).

$$\Delta\phi(n) = -\frac{2\pi n}{n_s} n_{120} = \pm 120^\circ \quad (20)$$

$$\Delta\phi(n) = -\frac{2\pi n}{n_s} n_{360} = 0^\circ \quad (21)$$

Summarizing, the harmonic components of the window signal, whose amplitude and phase are defined in (16) and (17), will appear in both the zero-sequence and the differential voltage, with exception of those that fulfil (20) for the zero-sequence voltage, and (21) for the differential voltage.

V. PARTIAL DEMAGNETIZATION FAULT DETECTION & QUANTIFICATION

A. Fault Detection

Previous section showed that the amplitude of some harmonic components of both the zero-sequence and the differential voltage depend on the PM demagnetization level. Thus, monitoring some specific harmonic components of the zero-sequence or the differential voltage will allow partial demagnetization fault detection.

B. Fault Quantification

Five different metrics for demagnetization level classification are considered: total energy, E (see (22)), energy of the largest harmonic component, E_{max} (see (23)), peak value of the signal, V^{peak} (see (24)), average of the absolute value of the signal, $|V|_{LPF}$, and total harmonic distortion, THD (see (25)), where $Y(n)$ is the amplitude of the harmonic component n . These metrics will be used both with the zero-sequence voltage and differential voltage.

$$E = \sum_{n=0}^{\infty} |Y(n)|^2 \quad (22) \quad E_{max} = |Y_{max}(n)|^2 \quad (23)$$

$$V^{peak} = \max(V) \quad (24) \quad |V|_{LPF} = LPF|V| \quad (25)$$

$$THD = \frac{E - E_{max}}{E_{max}} \cdot 100 \quad (26)$$

Fig. 5 shows the metrics as a function of M , for the pole pairs / slots combinations in Table IV and V; the results are normalized with respect to the case of $M = 0$ (i.e., full demagnetization). Normalization is required to make the results independent of machine design, i.e., rotor poles, stator slots, etc. It can be

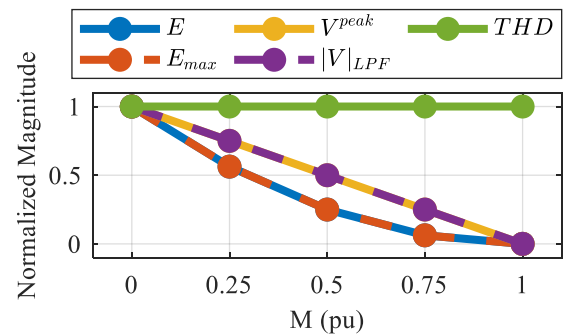


Fig. 5: Normalized total energy, E , energy of the largest harmonic component E_{max} , peak value, V^{peak} , average value of the absolute value, $|V|_{LPF}$ and THD depending on the demagnetization level, M , of both the zero-sequence and differential voltage, for all machine configurations shown in Table IV and V.

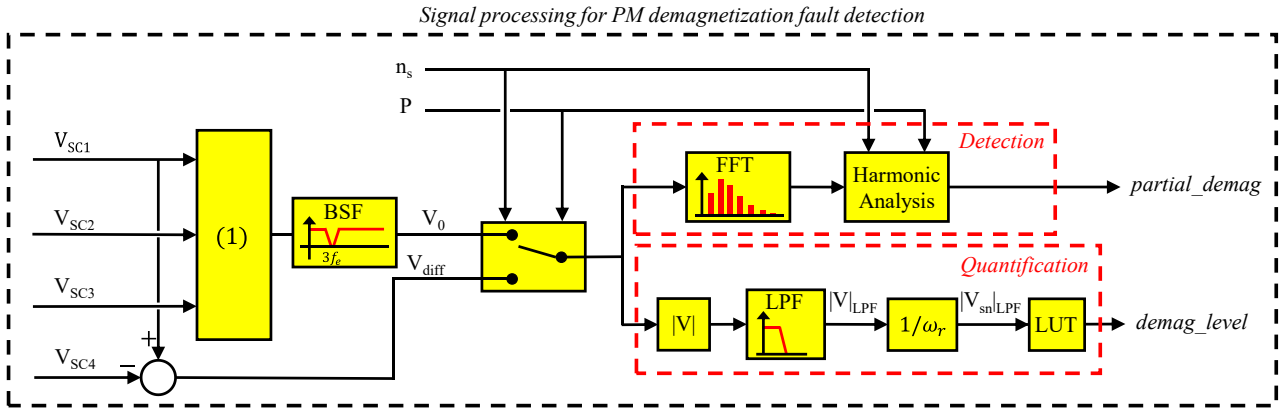


Fig. 6: Signal processing for PM demagnetization fault detection and quantification using both the zero-sequence voltage and the differential voltage.

observed from Fig. 5 that the THD is independent of M , partial demagnetization fault quantification being therefore not possible using this metric. On the other hand, E , E_{max} , V^{peak} , and $|V|_{LPF}$ increase with the demagnetization level (lower values of M). E and E_{max} are less sensitive to demagnetization than V^{peak} and $|V|_{LPF}$ at low demagnetization levels (values of M closer to 1), the tendency reverses at high demagnetization levels (values of M closer to zero). V^{peak} and $|V|_{LPF}$ exhibit constant sensitivity regardless M . It can be therefore concluded that V^{peak} and $|V|_{LPF}$ are the most suitable metrics since they show the highest sensitivity at low demagnetization levels. However, online measurement of V^{peak} could be difficult in practice e.g., due to noise. Thus, it can be concluded that $|V|_{LPF}$ is the most suitable metric for online partial demagnetization fault quantification.

VI. IMPLEMENTATION

The signal processing for demagnetization detection and quantification using the zero-sequence or the differential voltage is shown in Fig. 6. Two different stages are distinguished: (i) partial demagnetization fault detection and (ii) partial demagnetization fault quantification.

A. Fault Detection

Fault detection is based on monitoring specific harmonic components of V_0 and V_{diff} ; components between the DC and two times the fundamental frequency ($2 \cdot f_e$) will be monitored.

B. Fault Quantification

Use of V_0 or V_{diff} will depend on the machine configuration (see Tables IV and V). In case of using V_0 , a band stop filter (BPF) is required to remove the third harmonic component due to the non-sinusoidal BEMF shown by some PMSMs (especially SPMSMs). Then, after taking the absolute value of the signal, a 20Hz cut-off frequency low-pass filter will be used to obtain $|V|_{LPF}$. The resulting signal is divided by the rotating speed to make the measurement independent of speed, $|V_{sn}|_{LPF}$. Finally, a look-up table is used to obtain the demagnetization level, see Fig. 6.

VII. SIMULATION RESULTS

FEA simulations will be used for the validation of the proposed methods. Ansys Maxwell 2D will be used for this purpose. Figs. 7 and 8 show FEA results of the test machine (see Fig. 1 and Table III). Fig. 7a shows the induced voltage in SC-1, SC-2 and SC-3, while Fig. 7b shows the zero-sequence voltage.

Fig. 7c shows $|V|_{LPF}$ for the zero-sequence voltage. Fig. 7d shows the FFT of the zero-sequence voltage. It can be seen how the harmonic components obtained in simulation match with those ones predicted in Section IV, see Figs. 2f and 3f. Figs. 7e shows $|V_{sn}|_{LPF}$ vs. demagnetization level for the zero-sequence voltage, which will be used as look-up table for partial demagnetization fault quantification. Fig. 8 shows analogous results to Fig. 7 but for the differential voltage.

Fault detection and quantification process is represented in Figs. 9 and 10 both for V_0 and V_{diff} respectively. Fig. 9a shows the SC voltages, demagnetization fault appears at $t = 1s$; transition from 'no fault' ($t < 1s$) to 'fault' ($t > 1s$) condition being zoomed in Fig. 9b. Fig. 9c shows V_0 , its transition from 'no fault' to 'fault' condition being zoomed in Fig. 9d. Fig. 9e shows the fault detection signal 'partial_demag' (see Fig. 6). Fig. 9f shows the fault severity estimation signal, 'demag_level' (see Fig. 6). Steady state estimation errors are seen to be $< 4\%$, see Fig. 9g. Fig. 10 shows analogous results to Figs. 9 but for V_{diff} .

VIII. CONCLUSIONS

This paper proposes two different methods for PM demagnetization detection using SCs, namely: zero-sequence voltage-based and differential voltage-based. The feasibility of both methods has been shown to depend on machine design. It is concluded from the analysis presented in this paper that, for a given machine design, at least one of the two methods will be feasible. Harmonic components of both the zero-sequence and the differential voltage in the event of partial demagnetization have been obtained analytically. Methods for the processing of the signals, including quantification of the level of demagnetization, have been proposed. Simulation results have been shown to confirm the viability of the proposed methods. Experimental verification of the proposed methods is ongoing.

REFERENCES

- [1] J. Hong et al., "Detection and Classification of Rotor Demagnetization and Eccentricity Faults for PM Synchronous Motors," in IEEE Transactions on Industry Applications, vol. 48, no. 3, pp. 923-932, May-June 2012, doi: 10.1109/TIA.2012.2191253.
- [2] M. El Hachemi Benbouzid, "A review of induction motors signature analysis as a medium for faults detection," in IEEE Transactions on Industrial Electronics, vol. 47, no. 5, pp. 984-993, Oct. 2000, doi: 10.1109/41.873206.
- [3] D. Fernandez et al., "Permanent Magnet Temperature Estimation in PM Synchronous Motors Using Low-Cost Hall Effect Sensors," in IEEE Transactions on Industry Applications, vol. 53, no. 5, pp. 4515-4525, Sept.-Oct. 2017, doi: 10.1109/TIA.2017.2705580.

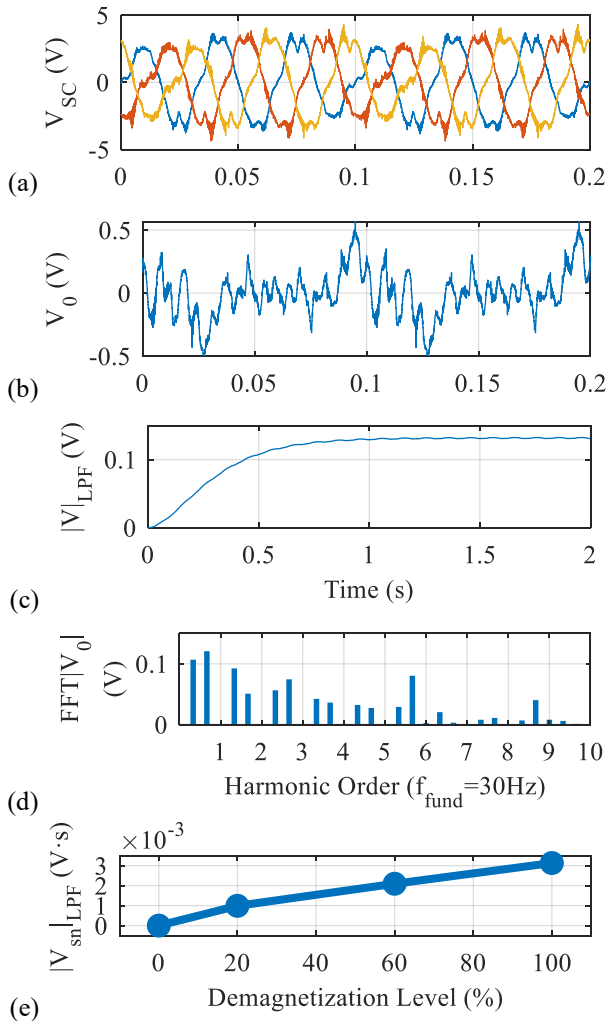


Fig. 7: (a) Individual SCs voltage, (b) zero-sequence voltage, (c) rectified and filtered zero-sequence voltage, (d) zero-sequence voltage FFT when PM1 is demagnetized (60%) and (e) average of the rectified zero-sequence voltage vs. PM demagnetization level. $I_{dq} = 0A$, $\omega_r = 600$ rpm.

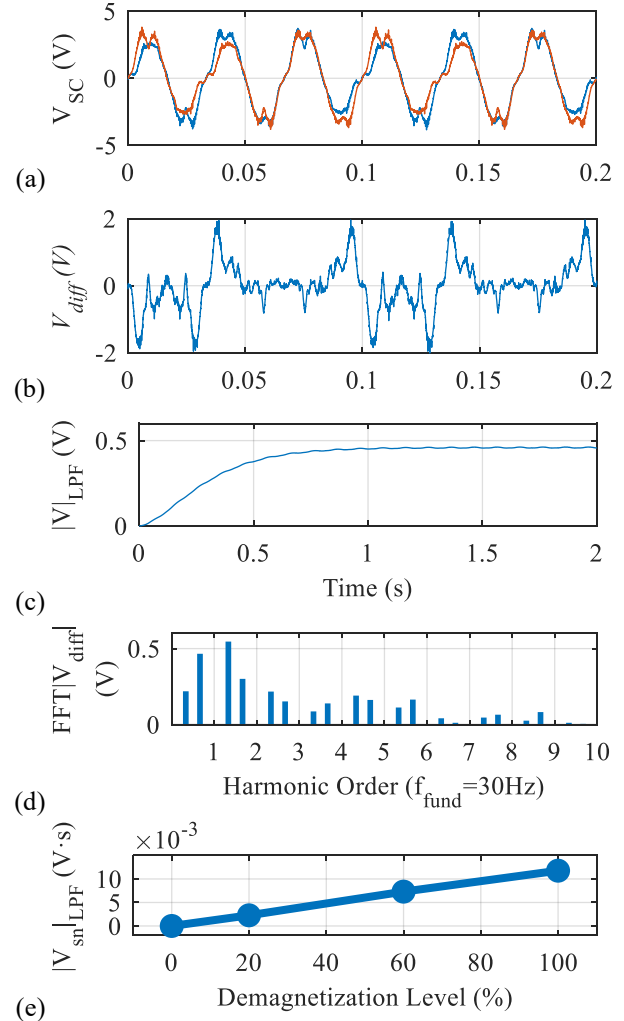


Fig. 8: (a) Individual SCs voltage, (b) differential voltage, (c) rectified and filtered differential voltage, (d) differential voltage FFT when PM1 is demagnetized (60%) and (e) average of the rectified differential voltage vs. PM demagnetization level. $I_{dq} = 0A$, $\omega_r = 600$ rpm.

[4] D. Reigosa, D. Fernández, M. Martínez, Y. Park, S. B. Lee and F. Briz, "Permanent Magnet Synchronous Machine Non-Uniform Demagnetization Detection Using Zero-Sequence Magnetic Field Density," in *IEEE Transactions on Industry Applications*, vol. 55, no. 4, pp. 3823-3833, July-Aug. 2019, doi: 10.1109/TIA.2019.2914892.

[5] Y. Park et al., "Online Detection of Rotor Eccentricity and Demagnetization Faults in PMSMs Based on Hall-Effect Field Sensor Measurements," in *IEEE Transactions on Industry Applications*, vol. 55, no. 3, pp. 2499-2509, May-June 2019, doi: 10.1109/TIA.2018.2886772.

[6] Y. Park et al., "Online Detection and Classification of Rotor and Load Defects in PMSMs Based on Hall Sensor Measurements," in *IEEE Transactions on Industry Applications*, vol. 55, no. 4, pp. 3803-3812, July-Aug. 2019, doi: 10.1109/TIA.2019.2911252.

[7] D. D. Reigosa, D. Fernandez, H. Yoshida, T. Kato and F. Briz, "Permanent-Magnet Temperature Estimation in PMSMs Using Pulsating High-Frequency Current Injection," in *IEEE Transactions on Industry Applications*, vol. 51, no. 4, pp. 3159-3168, July-Aug. 2015, doi: 10.1109/TIA.2015.2404922.

[8] D. Reigosa, D. Fernández, M. Martínez, J. M. Guerrero, A. B. Diez and F. Briz, "Magnet Temperature Estimation in Permanent Magnet Synchronous Machines Using the High Frequency Inductance," in *IEEE Transactions on Industry Applications*, vol. 55, no. 3, pp. 2750-2757, May-June 2019, doi: 10.1109/TIA.2019.2895557.

[9] D. Diaz Reigosa, D. Fernandez, Z. Zhu and F. Briz, "PMSM Magnetization State Estimation Based on Stator-Reflected PM Resistance Using High-Frequency Signal Injection," in *IEEE*

Transactions on Industry Applications, vol. 51, no. 5, pp. 3800-3810, Sept.-Oct. 2015, doi: 10.1109/TIA.2015.2437975.

[10] R. Hu, J. Wang, A. R. Mills, E. Chong and Z. Sun, "High-Frequency Voltage Injection Based Stator Interturn Fault Detection in Permanent Magnet Machines," in *IEEE Transactions on Power Electronics*, vol. 36, no. 1, pp. 785-794, Jan. 2021, doi: 10.1109/TPEL.2020.3005757.

[11] J. Penman, M. N. Dey, A. J. Tait and W. E. Bryan, "Condition monitoring of electrical drives," in *IEE Proceedings B - Electric Power Applications*, vol. 133, no. 3, pp. 142-148, May 1986, doi: 10.1049/ip-b.1986.0019.

[12] Y. Da, X. Shi and M. Krishnamurthy, "A New Approach to Fault Diagnostics for Permanent Magnet Synchronous Machines Using Electromagnetic Signature Analysis," in *IEEE Transactions on Power Electronics*, vol. 28, no. 8, pp. 4104-4112, Aug. 2013, doi: 10.1109/TPEL.2012.2227808.

[13] K. Ahsanullah, E. Jeyasankar, S. K. Panda, R. Shanmukha and S. Nadarajan, "Detection and analysis of winding and demagnetization faults in PMSM based marine propulsion motors," 2017 IEEE International Electric Machines and Drives Conference (IEMDC), Miami, FL, 2017, pp. 1-7, doi: 10.1109/IEMDC.2017.8002050.

[14] K. Ahsanullah, E. Jeyasankar, A. N. Vignesh, S. K. Panda, R. Shanmukha and S. Nadarajan, "Eccentricity fault analysis in PMSM based marine propulsion motors," 2017 20th International Conference on Electrical Machines and Systems (ICEMS), Sydney, NSW, 2017, pp. 1-6, doi: 10.1109/ICEMS.2017.8056162.

[15] S. M. Mirimani, A. Vahedi, F. Marignetti and R. Di Stefano, "An Online Method for Static Eccentricity Fault Detection in Axial Flux

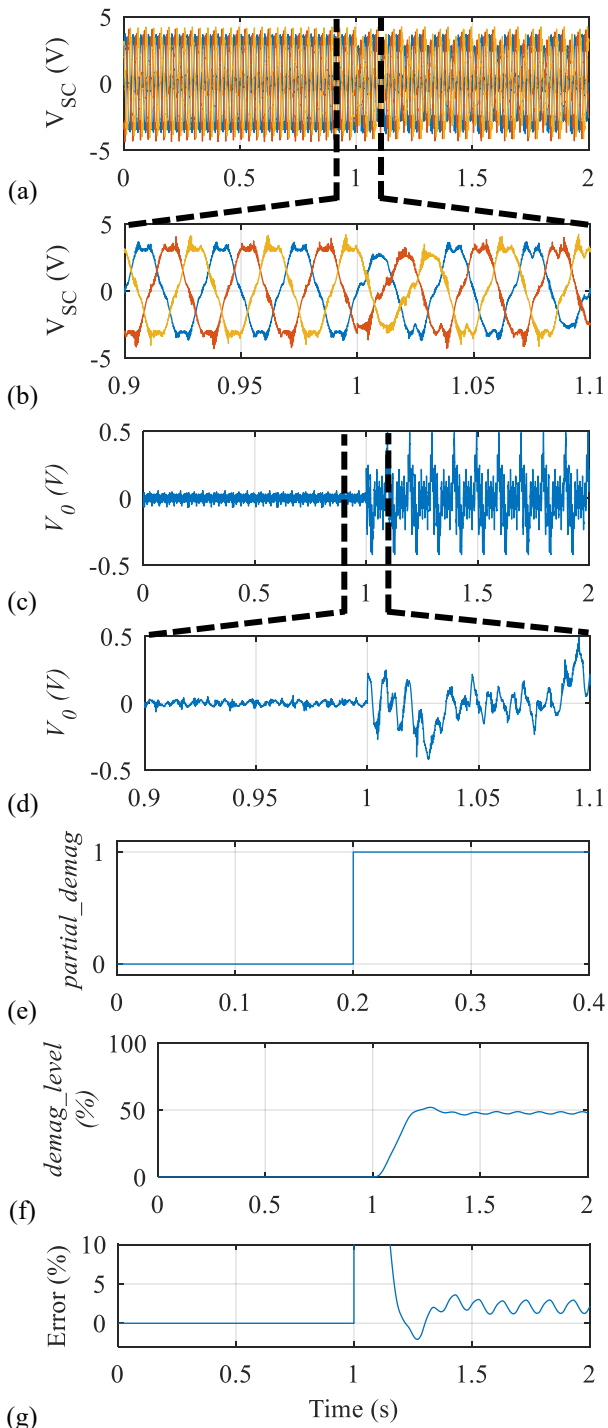


Fig. 9: (a) SC1, SC2 and SC3 voltage, (b) same as (a) but zoomed, (c) zero-sequence voltage, (d) same as (c) but zoomed, (e) fault detection signal, *partial_demag*, (f) fault quantification signal, *demag_level*, (g) fault quantification error. $t = 1$ s 50% partial demagnetization fault in PM1, $I_{dq} = \mathbf{0A}$, $\omega_r = 600$ rpm, *partial_demag*=0 meaning no fault, *partial_demag*=1 meaning demagnetization fault.

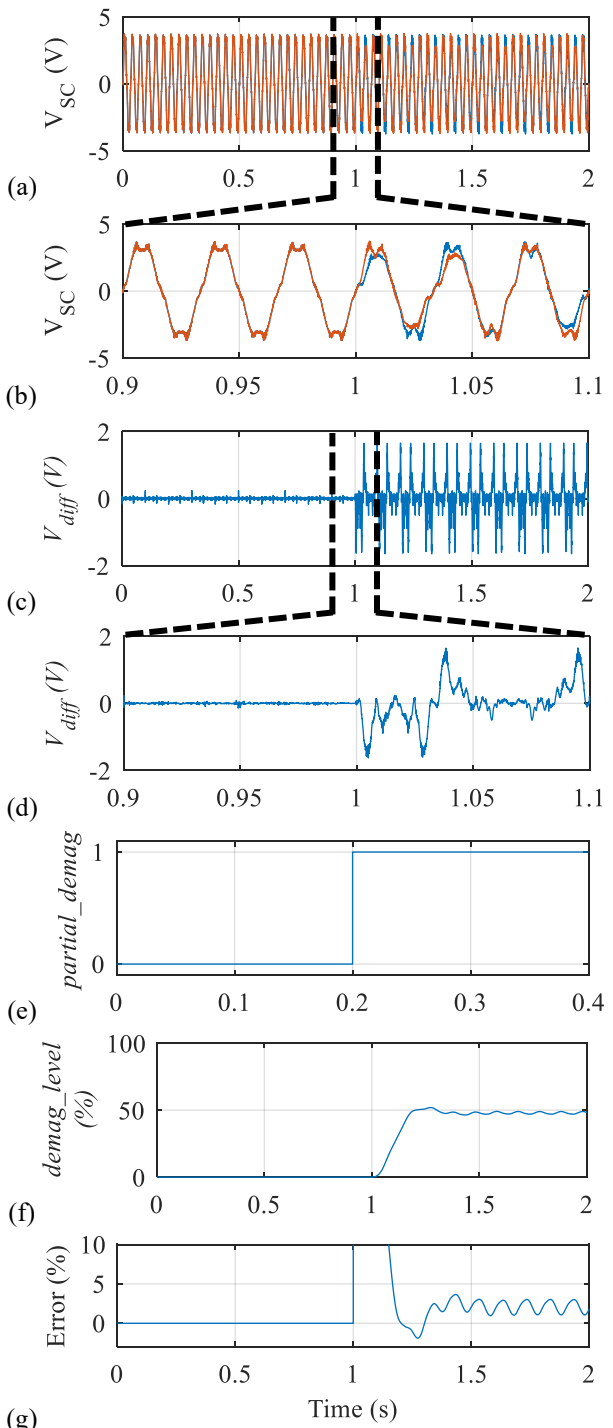


Fig. 10: (a) SC1 and SC4 voltage, (b) same as (a) but zoomed, (c) differential voltage, (d) same as (c) but zoomed, (e) fault detection signal, *partial_demag*, (f) fault quantification signal, *demag_level*, (g) fault quantification error. $t = 1$ s 50% partial demagnetization fault in PM1, $I_{dq} = \mathbf{0A}$, $\omega_r = 600$ rpm, *partial_demag*=0 meaning no fault, *partial_demag*=1 meaning demagnetization fault.

- Machines," in IEEE Transactions on Industrial Electronics, vol. 62, no. 3, pp. 1931-1942, March 2015, doi: 10.1109/TIE.2014.2360070.
- [16] K. Kang, J. Song, C. Kang, S. Sung and G. Jang, "Real-Time Detection of the Dynamic Eccentricity in Permanent-Magnet Synchronous Motors by Monitoring Speed and Back EMF Induced in an Additional Winding," in IEEE Transactions on Industrial Electronics, vol. 64, no. 9, pp. 7191-7200, Sept. 2017, doi: 10.1109/TIE.2017.2686376.
- [17] Y. Sui, J. Liu, Z. Yin, P. Zheng, L. Cheng and D. Tang, "Short-Circuit Fault Detection for a Five-Phase 30-Slot/32-Pole Permanent-Magnet Synchronous Machine," 2018 21st International Conference

on Electrical Machines and Systems (ICEMS), Jeju, 2018, pp. 50-54, doi:10.23919/ICEMS.2018.8549307.